Annals of Biomedical Engineering (2024) 52:208–225
https://doi.org/10.1007/s10439-023-03360-5

BMES BIOMEDICAL ENGINEERING SOCIETY

ORIGINAL ARTICLE

Reduced Order Modeling for Real-Time Stent Deformation Simulations of Transcatheter Aortic Valve Prostheses

Imran Shah[1,3] · Milad Samaee[1] · Atefeh Razavi[1] · Fateme Esmailie[1] · Francesco Ballarin[2] · Lakshmi P. Dasi[1] · Alessandro Veneziani[3,4]

Received: 29 March 2023 / Accepted: 1 September 2023 / Published online: 14 November 2023

Abstract

Computational modeling can be a critical tool to predict deployment behavior for transcatheter aortic valve replacement (TAVR) in patients with aortic stenosis. However, due to the mechanical complexity of the aortic valve and the multiphysics nature of the problem, described by partial differential equations (PDEs), traditional finite element (FE) modeling of TAVR deployment is computationally expensive. In this preliminary study, a PDEs-based *reduced order modeling* (ROM) framework is introduced for rapidly simulating structural deformation of the Medtronic Evolut R valve stent frame. Using fifteen probing points from an Evolut model with parametrized loads enforced, 105 FE simulations were performed in the so-called *offline* phase, creating a *snapshot* library. The library was used in the *online* phase of the ROM for a new set of applied loads via the proper orthogonal decomposition-Galerkin (POD-Galerkin) approach. Simulations of small radial deformations of the Evolut stent frame were performed and compared to full order model (FOM) solutions. Linear elastic and hyperelastic constitutive models in steady and unsteady regimes were implemented within the ROM. Since the original POD-Galerkin method is formulated for linear problems, specific methods for the nonlinear terms in the hyperelastic case were employed, namely, the Discrete Empirical Interpolation Method. The ROM solutions were in strong agreement with the FOM in all numerical experiments, with a speed-up of at least 92% in CPU Time. This framework serves as a first step toward real-time predictive models for TAVR deployment simulations.

Keywords Proper orthogonal decomposition · Model order reduction · Finite element analysis · Transcatheter aortic valve replacement · Predictive computational modeling

Introduction

Aortic stenosis (AS) is a widely prevalent valvular heart disease characterized by the narrowing of the aortic valve, located between the left ventricle and the aorta. AS is most often caused due to buildup of calcific deposits on the valve leaflets which restricts blood flow through the valve and to the systemic circulation, causing detrimental impact to the left ventricular function [48]. Although surgical aortic valve replacement (SAVR) has been the historical standard for treatment of AS, transcatheter aortic valve replacement (TAVR) has become an increasingly viable alternative to tackle severe AS, especially for high surgical risk patients who are unable to undergo traditional SAVR procedures [24]. Within the TAVR pre-procedural planning pipeline, there is a need for accurate assessment of potential complications that may arise after the TAVR procedure, such as coronary obstruction, paravalvular leakage, and leaflet

Associate Editor Umberto Morbiducci oversaw review of this article.

✉ Lakshmi P. Dasi
lakshmi.dasi@gatech.edu

✉ Alessandro Veneziani
ale@mathcs.emory.edu

[1] Wallace H. Coulter Department of Biomedical Engineering, Georgia Institute of Technology & Emory University, 387 Technology Circle, Atlanta, GA 30313, USA

[2] Department of Mathematics and Physics, Università Cattolica del Sacro Cuore, 48 Via Della Garzetta, 25133 Brescia, Italy

[3] Department of Mathematics, Emory University, 400 Dowman Drive, Atlanta, GA 30322, USA

[4] Department of Computer Science, Emory University, 400 Dowman Drive, Atlanta, GA 30322, USA

thrombosis [19, 37, 51]. Computational modeling via structural and fluid simulations has become a critical tool that can be used to visualize and predict deployment behavior mechanics for patient-specific TAVR procedures, and identify several post-TAVR complications [3, 14, 23, 26, 39, 41–43]. Such models can be used to assess the degree of paravalvular leakage in both traditional aortic valve replacement and specific abnormalities, such as bicuspid aortic valve disease, typically in a sequential manner with a structural simulation for modeling the valve deployment, followed by a fluid simulation to assess the degree of leakage [3, 13, 15, 26, 39, 43]. Alternatively, more comprehensive (and computationally expensive) modeling can be performed via a fluid–structure interaction (FSI) approach for quantifying flow surrounding the prosthetic valve following deployment at different heights and orientations [15, 36, 41].

Computational models are generally based on traditional numerical techniques for solving partial differential equations (PDEs) that underlie the fundamental mechanical problem. These numerical techniques generally may involve a representation of the approximate solution as a linear combination of functions with a finite number of coefficients. For instance, the displacement of the transcatheter valve frame under static conditions in TAVR deployment can be approximated by a linear combination in the following form,

$$\boldsymbol{u} = \left[u^{(j)}\right],\ j = 1,2,3, \quad \text{with}$$
$$u^{(j)}(x,y,z) = \sum_{i=1}^{N} u_{ij}\varphi_i(x,y,z), \quad i = 1,2,\ldots,N \tag{1}$$

where the coefficients u_{ij} are computed by solving an algebraic system of equations, and the basis functions $\varphi_i(x,y,z)$ can be selected in a variety of different ways. The Finite Element (FE) method is the most commonly used technique for the computational modeling of TAVR deployment, where these basis functions are local piecewise polynomials defined over the mesh elements [4, 30]. Popular FE solvers such as Abaqus FEA (SIMULIA, Providence, RI, USA) are based on this approach. In TAVR analysis, this requires modeling the transcatheter valve stent frame and leaflets, as well as the patient-specific aortic root, native leaflets, and calcium deposits. In this multi-component model, the intrinsic patient-specific geometrical complexities of each part call for fine meshes, potentially in the order of hundreds of thousands or even millions of elements [13]. This leads to a large number N of coefficients needed to accurately solve for the coefficients u_{ij} from the algebraic system of equations that arises from (1) and thus causes the process to be computationally expensive. Other complexities in TAVR analysis, including the nonlinear mechanical nature of the valve frame and leaflets, as well as the coupled interactions with the blood flow add to the computational costs [16]. Therefore, there is a need for rapid and accurate predictive models to assess patient-specific TAVR cases in daily clinical practice.

Several approaches have been proposed to help accelerate these TAVR analysis simulations. One such approach relies on optimizing the mesh utilized for these simulations, often in the form of 1-D beam elements or shell elements which have been shown to be much more computationally efficient as compared to traditional solid mesh elements [31]. Other approaches rely on constructing a fast surrogate model, for example, via a simplified geometrical description of the stent frame or a Machine Learning procedure (Gaussian Process) [9, 17]. In the present paper, we opted for a different approach where the surrogate model is still obtained by solving the PDEs of the problem, but with a specified educated basis function set that allows a strong reduction of the size of the discrete (numerical) problem. This approach goes under the general idea of "Model Order Reduction" [33]. In general, reduced order models (ROM) of this type refer to parameterized PDEs, i.e., PDEs featuring physical parameters or data whose values can be uncertain or change for our modeling purposes. Parameters can be in the constitutive law of a continuum, in the geometry or in the boundary conditions, like in the case of the present study. The construction of ROM often relies on the sequence of two primary steps, the *offline* and *online* stages. Computationally expensive simulations of the original parametrized Full Order Model (FOM) are performed in the offline stage for different values of the parameters. This creates a library of solutions or *snapshots*, from which low-dimensional reduced basis functions are formed for the rapid solution of the PDEs for any value of the parameters (in a physical range).

ROMs of this type have been employed in various cardiovascular applications to enhance and provide rapid cardiac simulations, including prediction of hemodynamics in patient-specific coronary artery grafts and estimation of arterial stiffness or cardiac conductivities in computational electrocardiology [8, 12, 49, 56, 58]. ROMs may play an especially significant role in performing real-time surgical planning simulations for a variety of different applications, largely due to their effectiveness in performing complex biomechanical simulations with a significantly reduced number of degrees of freedom [22]. Such approaches allow for near real-time evaluation of flow dynamics in patient-specific geometries [8, 58], as well as provide solutions to inverse problems that may generate critical information with regard to material properties and boundary conditions used in cardiac simulations [12, 49, 56]. Additional methods that follow the general idea of ROMs, such as reduced degree of freedom approaches, have been used for efficient hemodynamic simulations of bioprosthetic aortic valves as well [6]. However, the application of ROMs in predictive modeling

for TAVR deployment with regard to both the structural and fluid problem has not yet been studied in detail.

The primary objective of this study is to develop a ROM based on the so-called Proper Orthogonal Decomposition-Galerkin (POD-Galerkin) approach for the structural deformation of the Medtronic Evolut R (Medtronic Inc, Minneapolis, MN, USA) valve stent frame (26 mm), a self-expandable transcatheter heart valve (THV), where either a linear or hyperelastic constitutive law for the material is postulated. The development of this framework serves as a critical preliminary step toward real-time predictive models that encompass the entire TAVR deployment process. Such models may be used to provide clinically relevant information on potential post-TAVR complications in a real-time manner, as well as enhance and accelerate optimization analyses for patient-specific valve deployment simulations (i.e., understanding the effects of various valve types, positioning, etc.). Although this study utilizes the Evolut R valve, it should be noted that this framework is applicable to any THV. In fact, we have previously employed a similar ROM methodology for the CoreValve, and have begun adapting the framework for balloon-expandable valves. A rapid computation of the THV deformations is critical in any segregated method, or in general, iterative schemes where each step requires the solution of the problem several times and under different conditions. The focus here is on investigating the feasibility of the POD-Galerkin approach for rapidly simulating small structural deformations of the Evolut valve stent frame in response to a defined set of loads, which were applied radially inwards and outwards along different planes of the frame.

Materials and Methods

Equations

Let $\boldsymbol{u}$ denote the displacement vector of the region Ω (representing the Evolut R, as seen in Fig. 1). In order to assess the ability of our POD-Galerkin ROM, we will consider three different models, of increasing mechanical complexity:

1. The simplest problem considered in this preliminary study relies on a linear elastic constitutive law, and reads as: find $\boldsymbol{u}(x)$ such that

$$\nabla \cdot \boldsymbol{\sigma} = \mathbf{0}, \qquad \boldsymbol{x} \in \Omega, \tag{2}$$

where $\boldsymbol{\sigma} = \lambda(\nabla \cdot \boldsymbol{u})\boldsymbol{I} + 2\mu\boldsymbol{\varepsilon}$ is the Cauchy stress tensor and $\boldsymbol{\varepsilon} = \frac{1}{2}(\nabla \boldsymbol{u} + \nabla \boldsymbol{u}^T)$ is the strain tensor. $\boldsymbol{I}$ denotes the identity tensor. Finally, λ and μ are the Lamé constants. This linear constitutive law is a valid local approximation for small applied loads prescribed on the stent frame, resulting in small local deformations.
2. For larger deformations, such as those seen in traditional deployment simulations [4], nonlinear constitutive laws

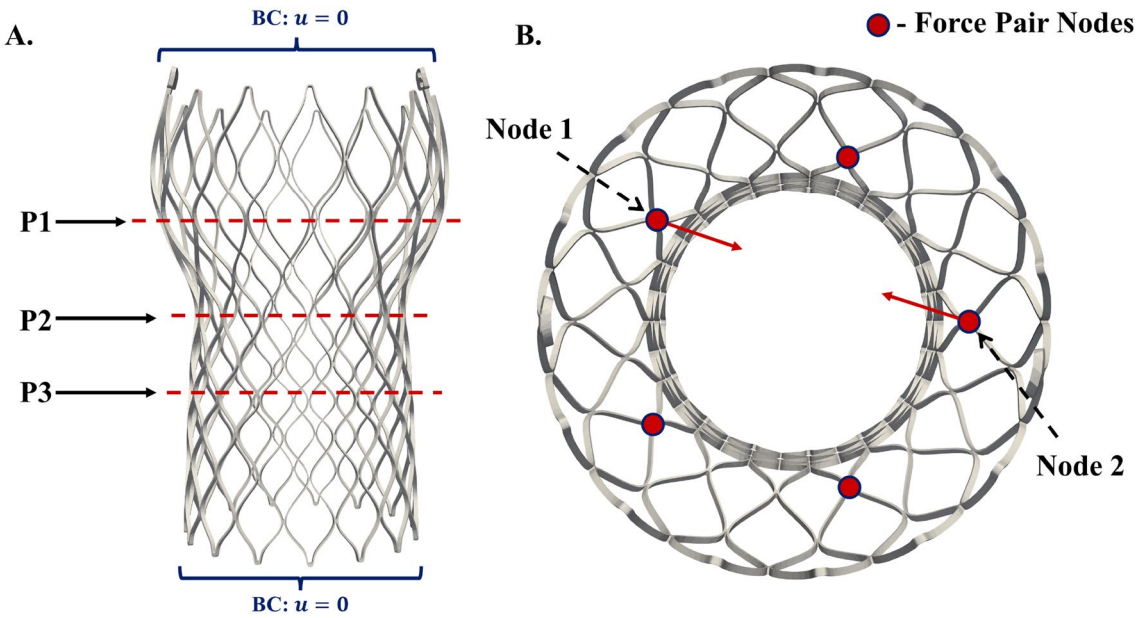

Fig. 1 **A** Idealized model of the Evolut R stent frame. The fixed edges of the stent are shown, as well as the three planes P1, P2, and P3 along which all force-pair boundary conditions are prescribed at fifteen specified nodes. **B** Five nodes at which force-pair conditions are applied at one of the planes, and sample force-pair boundary condition applied between two nodes of the stent frame. The force applied at each node (in red for the online version of the paper) is equal and opposite to one another

are required to accurately capture the deformation of the self-expandable nitinol frame of the valve. For this aim, a superelastic behavior as presented by Auricchio et al. [5] is needed, and previous studies have emphasized the importance of the superelastic material parameters for modeling the mechanical response of self-expandable nitinol THVs [18]. We consider here a hyperelastic constitutive law as a first step toward capturing the highly nonlinear nature of the superelastic constitutive model. The basic approach for the proposed hyperelastic model is the minimization of the strain energy density function

$$\psi = \frac{\mu}{2}(I_c - 3) + \frac{\lambda}{2}(J-1)^2, \tag{3}$$

where if the right Cauchy-Green deformation tensor is denoted as $\boldsymbol{C} \equiv \boldsymbol{F}^T\boldsymbol{F}$, J is the Jacobian of the deformation gradient, i.e., $J = \det(\boldsymbol{F})$, and I_c is its first invariant (trace). The stress–strain relationship then reads as follows, in Cartesian tensor form:

$$\boldsymbol{\sigma}_{ij} = \frac{\mu}{J^{5/3}}(\boldsymbol{C}_{ij} - \frac{1}{3}\boldsymbol{C}_{kk}\boldsymbol{\delta}_{ij}) + \frac{\lambda}{2}(J-1)\boldsymbol{\delta}_{ij}. \tag{4}$$

3. The previous models are based on the steady forms of the linear and hyperelastic constitutive laws. As a third and final model, we considered the time-dependent hyperelastic problem to assess our approach for transient structural problems. In this case, the problem in (2) is modified to include the acceleration term as follows.

$$\rho\frac{\partial^2\boldsymbol{u}}{\partial t^2} + \nabla\cdot\boldsymbol{\sigma} = 0 \tag{5}$$

The problem needs to be completed with boundary conditions, and in the the transient problem initial conditions as well. The boundary of the domain $\partial\Omega$ was split into three conceptual non-overlapping parts whose union forms the whole boundary for both the linear elastic and hyperelastic problems. In the first part, at the lower and upper surfaces of the stent frame (for $z = 0$ and $z = 55$ mm), the displacement was set as $\boldsymbol{u} = \boldsymbol{0}$, which assumes that the stent is undeformed at the extremes (Fig. 1). This choice is a simplification, as in more realistic scenarios we may need to prescribe conditions related to the contact of the stent with other surfaces; however, it is worth noting that for the purpose of the model reduction, these conditions are expected to have a minor impact.

In the second part, at a set of 15 points distributed across three different planes of the Evolut stent frame (Fig. 1A, B), it was assumed that the normal stress was given, i.e., $\boldsymbol{\sigma}\cdot\boldsymbol{n}\left(P_i\right) = \boldsymbol{d}_i$, for $i = 1, 2, \ldots, 15$, where $\boldsymbol{n}$ is the outward normal unit vector. More precisely, all possible pairs among the fifteen points were selected, and $\boldsymbol{d}_i$ was defined as a vector oriented along the line connecting the two endpoints of each pair as seen in Fig. 1B. The number of possible pairs is given by the binomial coefficient $\binom{15}{2} = 105$. Each of these "force-pair" boundary conditions may be used to idealize the applied loads from the aortic wall and prosthetic leaflets onto the deployed configuration of the valve stent frame. These force-pair conditions also serve as an initial step toward replicating the forces the stent frame undergoes during traditional crimping and expansion simulations performed in previous computational TAVR studies, with the goal of eventually replicating the cylinder used in such studies via the use of these force-pair conditions. However, further refinements of these conditions will be needed to fully capture the traditional methods (i.e., the cylindrical catheter) used in many previous FE-based TAVR studies [4, 41, 55]. Here, these pairs represent the parameterization of the given problem, to be eventually reduced via the POD approach.

For the remaining boundary, homogeneous Neumann boundary conditions were applied, i.e., $\boldsymbol{\sigma}\cdot\boldsymbol{n} = \boldsymbol{0}$. These conditions, in fluid mechanics, are sometimes advocated as "do-nothing" conditions as they are the conditions to prescribe in the absence of specific data and occur naturally in the variational formulation of the problem without adding any specific term [34]. These same boundary conditions were used for the steady linear elastic and hyperelastic simulations. In the case of the transient hyperelastic problem, time-dependent BCs were also implemented to test the capabilities of the proposed ROM for tackling truly transient problems. In particular, the applied forces for the second part of the boundary were modulated by a sinusoidal function in time to describe varying magnitudes. An initial condition in the form of $\boldsymbol{u} = \boldsymbol{0}$ is employed as well.

The ROM Framework

The ROM framework, divided into *offline* and *online* stages, is illustrated in Fig. 2. There are two common approaches that can be pursued for the offline stage. In the greedy Reduced-Basis method, the snapshots are created by solving the FOM for specific values of the parameters that maximize the level of information brought by a new snapshot. The identification of these values requires *a posteriori* estimates that for general problems like the hyperelastic case are not readily available. For this reason, we opted for the other approach. In the POD approach, the parameter space is, in general, over-sampled uniformly to create a library. This library is oversized, in the sense that each snapshot is solving the same problem under different conditions and carries information partially overlapping with the other snapshots. Filtering the redundancy is critical to obtain an efficient ROM. This step is carried out by means of a well-known linear algebra tool, the *Singular Value Decomposition*

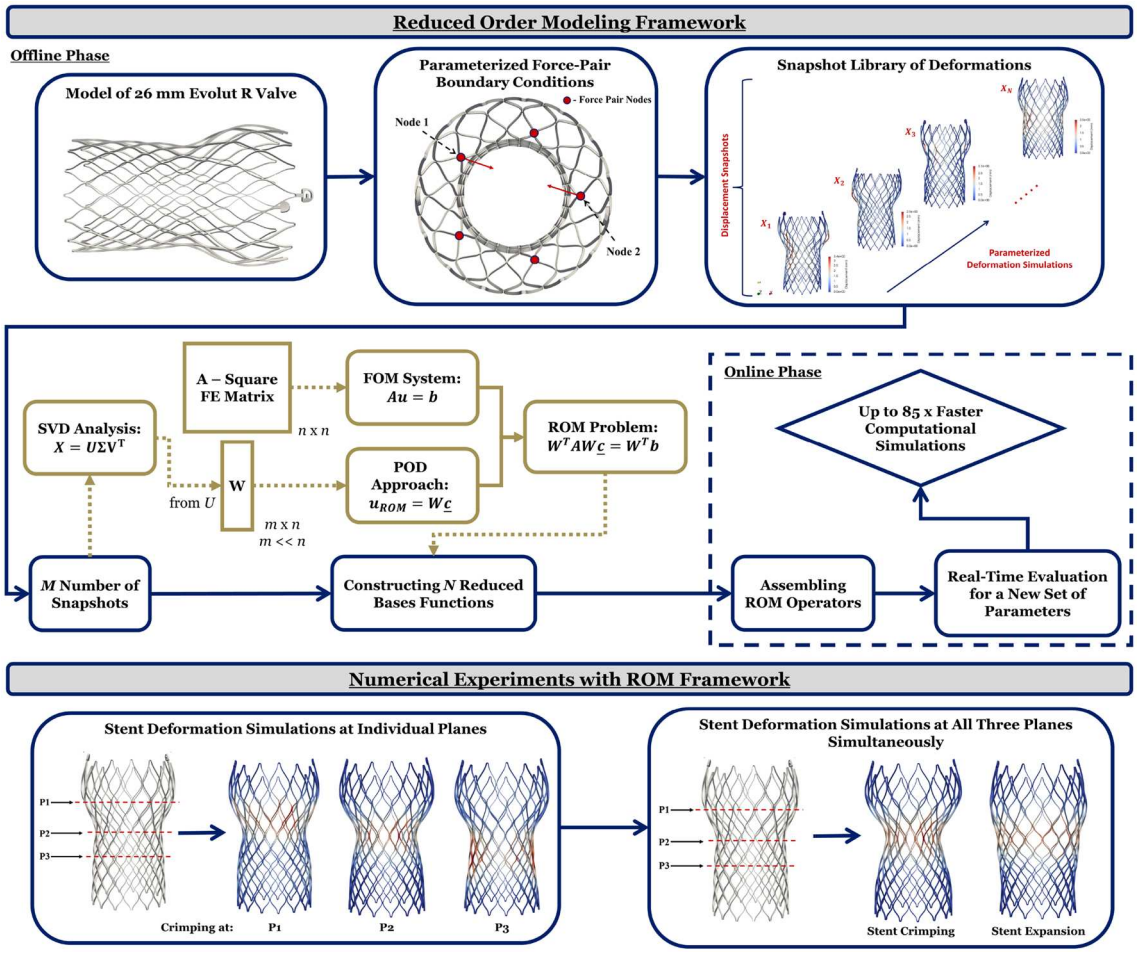

Fig. 2 Summary of the reduced order modeling (ROM) framework and the numerical experiments performed with the ROM. The framework can be split into an offline phase, where the computationally expensive simulations are offloaded, and an online phase, where they are promptly recycled for a new set of parameters to obtain a reduced order solution

(SVD). Using this tool, a low-dimensional basis function set is constructed and the original physical problem is projected to the function space given by the linear combinations of these functions. The online stage consists of the solution of this low-dimensional problem for any given value of the parameters.

Offline Phase

The 3D geometry of the valve utilized was a model of the 26 mm Medtronic Evolut R stent frame. The stent frame was generated in *SolidWorks* (Dassault Systems, Concord, MA, USA), and meshed with first-order tetrahedral elements (270 K) using the open-source platforms *Netgen/NGSolve* (Vienna University of Technology, Vienna, Austria, https://ngsolve.org/) and *Mmg Platform* [45]. Although such a mesh size allows for accurate deformation results, structured grids in the form of hexahedral meshes have been previously shown to be more efficient in the context of stent deformations and THV deployment simulations [27, 30, 31]. However, due to limitations within the FE solvers used which are unable to efficiently handle hexahedral meshes (see Supplemental Materials Section D for additional details), a tetrahedral mesh was chosen for this study. To optimize the tetrahedral mesh, a convergence study was performed. Hyperelastic deformation simulations with mesh sizes ranging from 16,000 to 800,000 tetrahedral elements were performed and the resultant stresses and computational costs were calculated, with detailed results available in the Supplemental Materials Section D. This analysis resulted in the final mesh size of 270 K tetrahedral elements utilized in the remainder of the study. Furthermore, the use of quadratic Lagrange basis functions for tetrahedral meshes has been shown to be equally as efficient or better than hexahedral elements in the context of elliptical PDEs (i.e., Neo-Hookean elasticity) [52]. Numerical experiments were performed with linear and quadratic Lagrange basis functions, highlighting the effectiveness of the proposed ROM framework in

reducing computational costs of stent deformation simulations, regardless of the element type utilized (Supplemental Materials Section F).

The *Mmg Platform* was specifically used to refine mesh elements at localized regions near the intersection of the stent struts, where the original mesh elements may become distorted. As seen in Fig. 1A, the idealized model of the Evolut R does not include the porcine pericardium-based leaflets and skirt. This simplification of the model enabled the ROM framework to solely focus on the stent deformation as a first step toward fully capturing the THV deployment. The Evolut R stent frame was modeled with both linear elastic and hyperelastic material properties as defined previously, with Young's modulus of 50 GPa and Poisson's ratio of 0.33 [27]. For the *offline stage*, linear and hyperelastic FE simulations were performed with the Evolut R stent frame. All simulations were performed using an in-house solver built in *FEniCS*, an open-source FE library [2, 40]. Details on the FE formulation for both cases are provided in the Supplemental Materials Section A. For the transient hyperelastic simulations, an implicit time-advancing scheme is introduced to iterate and solve for each time step, to promptly linearize the governing transient nonlinear problem. Here, the time step was defined as 0.01 s, and the total time simulated was 0.3 s. These values were chosen as an initial approximation of the total time taken for the stent to undergo crimping and expansion during deployment.

With 15 nodes across the stent geometry to parameterize the boundary conditions, a total of 105 offline stage simulations were conducted. A sample force-pair between two nodes of the stent frame is shown in Fig. 1B. During this "training" phase, the magnitude of the applied loads for each of the 105 FE simulations was randomly sampled from a range of 0–10 Newtons (N). This range was chosen as an initial approximation of the radial forces that may be produced on the anatomical tissue due to implantation of such self-expandable prostheses, as well as the physiological forces applied to the deployed stent frame that may potentially dislodge the prosthesis, which have been quantified in previous computational and in vitro experimental studies [44, 47, 53]. Small radial deformations of the Evolut R stent frame were simulated at the three planes P1, P2, and P3 as shown in Fig. 1A via these force-pairs to form a *snapshot* library.

Singular Value Decomposition of the Snapshots

The generated snapshots are a representation of the solution to the problem under different boundary conditions. While each snapshot represents a different solution, the level of information each carries about the solution of the problem under different conditions is generally redundant. The final goal is to construct a set of functions to use for the rapid computation of the online problem by taking advantage of this library; however, the efficiency of the method relies on effective filtering of this redundancy. To do this, the SVD is employed [50, 54]. The SVD states that given a generic $m \times n$ matrix B, it is possible to factorize it into three matrices as follows,

$$B = W\Sigma V^T, \tag{6}$$

where W is an $m \times m$ orthonormal matrix (i.e., $W^T W = I$) whose columns are known as the left-singular vectors of B (corresponding to the eigenvectors of BB^T), V is an $n \times n$ orthonormal matrix whose columns are the right-singular vectors of B (corresponding to the eigenvectors of $B^T B$), and Σ is a $m \times n$ diagonal matrix whose entries contain the singular values. The singular values Σ are non-negative and ordered in decreasing fashion. They represent the importance of the corresponding eigenvectors in the linear space formed by the snapshots. A rapid decay in the singular values indicates high redundancy in the snapshot matrix, and that the key features of the snapshot matrix can be captured by a linear combination of those left eigenvectors associated with the largest singular values [20]. Consequently, a fast decay in the singular values suggests that the number of degrees of freedom may be significantly reduced as the snapshots are redundant.

The 105 snapshots describe the displacement for each of the offline simulations in the nodes of the mesh. These snapshots were organized in a matrix B and the SVD of B was computed. Once computed, the largest singular values were identified according to the criterion

$$\frac{\sigma_k}{\sigma_0} \geq \vartheta,$$

where σ_0 is the largest singular value and ϑ is a user defined cut-off parameter. Let n_{ROM} denote the number of singular values that fulfill the condition; all singular values that do not fulfill the cut-off condition were subsequently discarded. The model reduction consists in selecting the left eigenvectors $\boldsymbol{w}_i$, columns of W, associated with the singular values maintained by the procedure. These eigenvectors form the reduced order basis in the sense that the ROM solution reads as

$$\boldsymbol{u}_{ROM} = \sum_{i=1}^{n_{ROM}} c_i \boldsymbol{w}_i = W\boldsymbol{c}, \tag{7}$$

where W is an $N \times n_{ROM}$ matrix. The coefficients $\boldsymbol{c}$ are found by solving the reduced problem as described in the following section. An alternate approach to calculating the SVD that was initially implemented is discussed in the Supplemental Materials Section B.

The Proper Orthogonal Decomposition-Galerkin Approach

After discretization of the problem, the FOM from (2) and (5) leads to the solution of a linear system in the form

$$A\boldsymbol{u} = \boldsymbol{b} \tag{8}$$

where $\boldsymbol{u}$ denotes the vector of displacements, A is the system matrix, and $\boldsymbol{b}$ collects the effects of the forcing terms and boundary conditions. The matrix A is indeed the stiffness matrix for the steady linear elasticity case, while it results from linearization of nonlinear terms in the hyperelastic problem. For the sake of notation, in the transient case, A also includes the mass term due to the time derivative term, and $\boldsymbol{b}$ additionally incorporates its application to the solution at the previous time step. In the POD-Galerkin approach, an approximate solution in the form of (7) is postulated, after having computed W during the offline phase. By plugging this form into the discrete problem (8) and following the Galerkin procedure (representing the testing functions also as columns of W), the following reduced system is obtained:

$$W^T AW\boldsymbol{c} = W^T\boldsymbol{b}. \tag{9}$$

In (9), $W^T AW$ is a $n_{ROM} \times n_{ROM}$ matrix, where n_{ROM}, in general, features a size in the range of tens or hundreds of rows. Using (9) with the vector $\boldsymbol{b}$ incorporating the new boundary conditions of interest in the online stage, the "small" vector $\boldsymbol{c}$ can be found from (7), from which the final reduced order solution can be solved for. The savings in computational costs become evident when comparing the sizes of the A in Eq. (8) to the reduced order matrix $W^T AW$ in (9). Furthermore, since the action of the parameters only affects the right-hand side $\boldsymbol{b}$, the matrix $W^T AW$ can be precomputed once and for all at the end of the offline stage. Solving the reduced order problem requires much fewer degrees of freedom compared to the full order FE problem, and thus results in significantly reduced computational costs.

The Nonlinear Problem The Galerkin POD approach is naturally stated for linear problems. In the case of nonlinear problems, like for the hyperelastic case, specific approximation techniques are required. We resorted here to a technique called Discrete Empirical Interpolation Method (DEIM), see [11, 21, 33]. The DEIM approach allows for efficient reduction of the nonlinear terms that arise in the hyperelastic problem, which the traditional POD approach is unable to reduce effectively since it would not be possible to precompute $W^T AW$ once and for all, as A itself depends on the solution at the previous nonlinear iteration. The DEIM approach was utilized for both the steady and time-dependent hyperelastic problem. Additional details with regard to the DEIM algorithm are included in the Supplemental Materials Section E.

Software Tools and Libraries

To perform the model reduction approach described above, several libraries were used beyond the geometrical and meshing libraries NGSolve (Netgen) and MMGTools already mentioned. The model reduction was carried out by using the library *RBniCS*, an open-source model reduction library (https://www.rbnicsproject.org/ [33]). This is based on *FEniCS*, a Python-C++ library for finite element computations.The entire problem is managed by the library, from the offline phase to the model reduction as well as the speed-up analysis. Most of the simulations were performed on a local laptop (Dell XPS 15, with 8 Intel Core H-series i9-11900 H "Tiger Lake" 2.5 GHz Sixteen Core 10nm CPU, 32GB Total Memory, 1TB Storage). A workstation (Microway WhisperStation, with 12 Intel Core X-series i7-7800X "SkyLake" 3.50 GHz Six Core 14nm CPU, 64GB Total Memory, 10TB Storage) was used only for the offline phases of the steady and transient hyperelastic POD-DEIM problems. while all the online computations were done on the laptop, highlighting the translatability of the approach for use in commonly seen computers in the clinical environment. The workstation was needed mainly for the memory required for computing the additional steps that are introduced with the DEIM algorithm (secondary SVD and interpolation matrix computation), and is further discussed in the Supplemental Materials Section E. Finally, visualization of all results was done with *ParaView* (Kitware Inc., Clifton Park, NY, USA) [1].

In the case of linear elasticity, the results of the library were cross-validated by a manual approach, performed by the authors combining *FEniCS* for the snapshot generation and *MATLAB* (MathWorks, Natick, MA, USA) for the SVD computation. The results obtained in the two ways agree, and thus results obtained from this cross-validation are omitted from the presentation hereafter.

Numerical Experiments

The ROM framework described above was applied in two different numerical experiments as summarized in Fig. 2. In each scenario, the same procedure for setting up the ROM framework is followed, i.e., utilizing the force-pair conditions at a pair of 15 nodes across three different planes of the stent geometry to parameterize the problem, creating a snapshot library, performing the SVD analysis, and employing the POD-Galerkin approach for model reduction.

1. First, we investigated the applicability of the ROM framework for small structural deformations of the Evolut stent frame at each of the three individual planes *P1*, *P2*, and *P3* using radially inward and outward applied forces. The magnitude of the applied loads enforced in

the online stage ranged from 3 to 5 N in this case for the plane at which the deformation occurs. These simulations were performed as test cases with only the linear elastic material properties to confirm that the force-pair boundary conditions were working as expected (i.e., deforming the stent inwards and outwards).

2. Second, the radially inward and outward forces were applied at all three planes *P1*, *P2*, and *P3* simultaneously, with the magnitudes of the applied loads utilized in the online stage ranging from 4 to 7 N. These simulations were performed using both the linear and hyperelastic constitutive laws in the steady and transient regimes, and served as a more complex application of the developed ROM framework. Here, these conditions are used to simulate idealized crimping and expansion of the stent frame along the mentioned planes. More importantly, they serve as an initial investigation into the feasibility of using such an ROM framework for simulating the full crimping and deployment of the Evolut stent frame.

Results

In the following sections, we present the results of the SVD algorithm on the snapshot library generated from the offline phase. Results from the numerical simulations generated via the ROM with newly defined boundary conditions (i.e., not included in the snapshot library) are also presented, which are compared to FE simulations with the same applied boundary conditions. Reduction in the degrees of freedom and computation time between the FOM and ROM are summarized as well.

Results of the Singular Value Decomposition

The singular values σ_j for the stent frame deformation in the linear elastic simulations are plotted and are shown in Fig. 3A, as function of their index j. A sharp and rapid decline in the eigenvalues is seen, at approximately 13 reduced bases, suggesting that the entire FOM can be well approximated by the left eigenvectors associated with the first 13 principal components of the snapshot library. In addition, the retained energy calculated for each reduced bases utilized is also plotted for the linear elastic case in 3A. The plot plateaus at 13 reduced bases, which corresponds to 99.99 % of the energy captured from the snapshot library. This suggests that in the linear case, the 13 reduced bases can be used to construct the reduced basis functions and calculate the reduced order solution. In the case of hyperelasticity, the eigenvalue decay and retained energy are also plotted in 3B. Here, a sharp decline in the eigenvalues is again seen, this time at approximately 20 reduced bases. The retained energy also indicates that the first 20 reduced bases capture

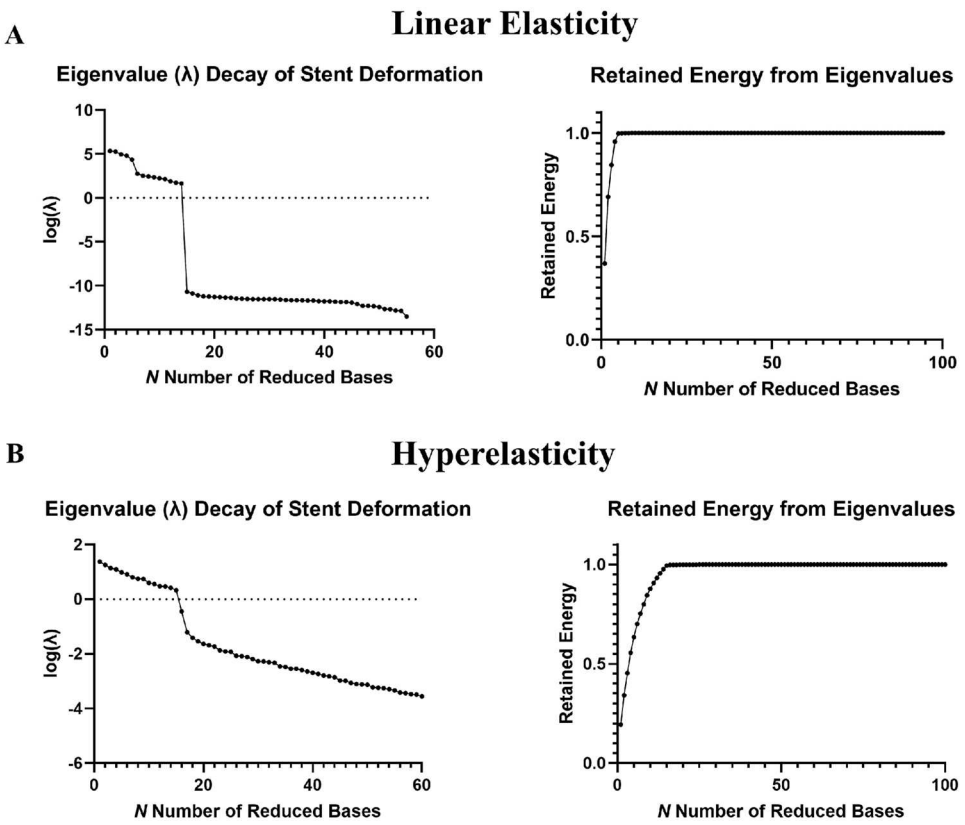

Fig. 3 Eigenvalue decay and retained energy calculated for each number *N* of reduced bases captured, for linear elastic simulations (**A**) and hyperelastic simulations (**B**)

99.99 % of the energy from the hyperelastic deformations. Thus, for the hyperelastic case, using the 20 reduced bases is sufficient to continue the remaining POD steps.

ROM vs FOM Solutions

Two distinct types of simulations are reported: first, small structural deformations of the Evolut stent frame in response to radially inward and outward applied forces along each of the three individual planes $P1$, $P2$, and $P3$ were performed. These sets of simulations were conducted with linear elastic governing mechanics as described previously to confirm that the force-pair boundary conditions are working as intended. They are labeled as follows: Case I for radial forces applied along $P1$, Case II for radial forces applied along $P2$, and Case III for radial forces applied along $P3$. Second, we report ROM and FOM simulations with the radially applied forces at all three planes simultaneously, which may serve as an initial step toward capturing the crimping and expansion process of the stent frame. These simulations were performed with both the linear elastic and hyperelastic constitutive models.

Deformations of the Evolut R stent frame in response to radially inward applied forces (labeled as stent crimping) with linear elastic properties using the ROM framework and the FOM FE simulations are shown in Fig. 4A–C for three distinct cases. In the three cases, force boundary conditions were applied to face radially inwards across P1, P2, and P3 individually. For all cases, a strong agreement was seen between the resultant deformations of the ROM and FOM solutions. In the first case, the maximum deformation in the ROM solution was 1.688 mm, while the maximum deformation in the FOM solution was 1.684 mm at the same node (Fig. 4A). In the second case, the maximum deformation was 2.394 mm for the ROM solution compared to 2.393 mm for the FOM solution (Fig. 4B), both at the same node. Finally, in the last case, the maximum deformation was 1.279 mm for both the ROM solution and the FOM solution (Fig. 4C). When solving for the full order problem, 210,417 degrees of freedom were attained, and after the application of the model reduction techniques, the number of degrees of freedom was reduced to 13 in total for Cases I and II and 12 for Case III.

The expansion of the Evolut R stent with linear elastic properties using the ROM and the FOM for three similar cases is shown in Fig. 4D–F. In this scenario, boundary conditions are prescribed as radially outwards (labeled as stent expansion) at P1, P2, and P3 individually. In all three cases, strong agreement was again seen between the ROM and FOM solutions. The ROM solution in Case I resulted in a maximum deformation of 1.690 mm; the FOM solution resulted in a maximum deformation of the same value at the same node as in the ROM (Fig. 4D). For Case II, the maximum deformation for the ROM solution was 2.389 mm and for the FOM solution was 2.386 mm (Fig. 4E). Finally, in Case III, the maximum deformation in the ROM solution was 1.291 mm and in the FOM solution was 1.290 mm (Fig. 4F). The degrees of freedom for the FOM, the number of reduced bases formed during the ROM were the same as reported in the previous cases.

The average error and average relative error between the ROM and the FOM solutions over each of the reduced bases were calculated for all stent crimping cases and are plotted in Fig. 5A, B. Crimping along P1 resulted in the average error decreasing from 43.955 to 0.505 as the number N of reduced bases in the ROM increased from 1 to 13 (Fig. 5A—Case I), while the average relative error decreased from 0.734 to 0.008 (Fig. 5B—Case I). For crimping along P2, the average error decreased from 53.736 to 0.361 (Fig. 5A—Case II) over the same number of reduced bases, while the average relative error decreased from 0.759 to 0.005 (Fig. 5B—Case II). The average error decreased from 78.875 to 0.962 for crimping along P3 (Fig. 5A—Case III) as the number of reduced bases increased from 1 to 12, and average relative error decreased from 0.745 to 0.009 (Fig. 5B—Case III).

Average error plots for all stent expansion simulations are shown in Fig. 5C, D. The average error decreased from 43.128 to 0.394 for Case I as the number of reduced bases increased from 1 to 13 (Fig. 5C—Case I), and the relative error decreased from 0.763 to 0.007 (Fig. 5D—Case I). In Case II, the average error decreased from 53.807 to 0.472 over the same number of reduced bases (Fig. 5C—Case II), and relative error decreased from 0.789 to 0.007 (Fig. 5D—Case II). For Case III, the average error decreased from 74.594 to 0.856 as the number of reduced bases increased from 1 to 12 (Fig. 5C—Case III), and the relative error decreased from 0.724 to 0.008 (Fig. 5D—Case III).

The final set of simulations applies radially inward (crimping) and outward (expansion) boundary conditions at all three planes simultaneously, for both linear and hyperelastic material properties. With a linear elastic model, crimping of the Evolut stent frame at all three planes is shown in Fig. 6A. Maximum deformation in both the ROM and FOM simulations was 3.985 mm (central plane of the stent). In the case of expansion (Fig. 6B), the maximum deformation for both the ROM and FOM was 5.533 mm, while the rest of the frame deformed similarly. The average error and relative error for these cases were similar in magnitude to the deformations along the individual planes shown previously. The number of reduced bases utilized increased to 15, compared to 12 and 13 reduced bases from previous simulations. It is worth noting that the fact that the error falls significantly with 15 degrees of freedom is expected for the linearity of the problem since the superposition of effects holds. While we expect the number of degrees of freedom of the reduced model to increase in the nonlinear case, we anticipate this

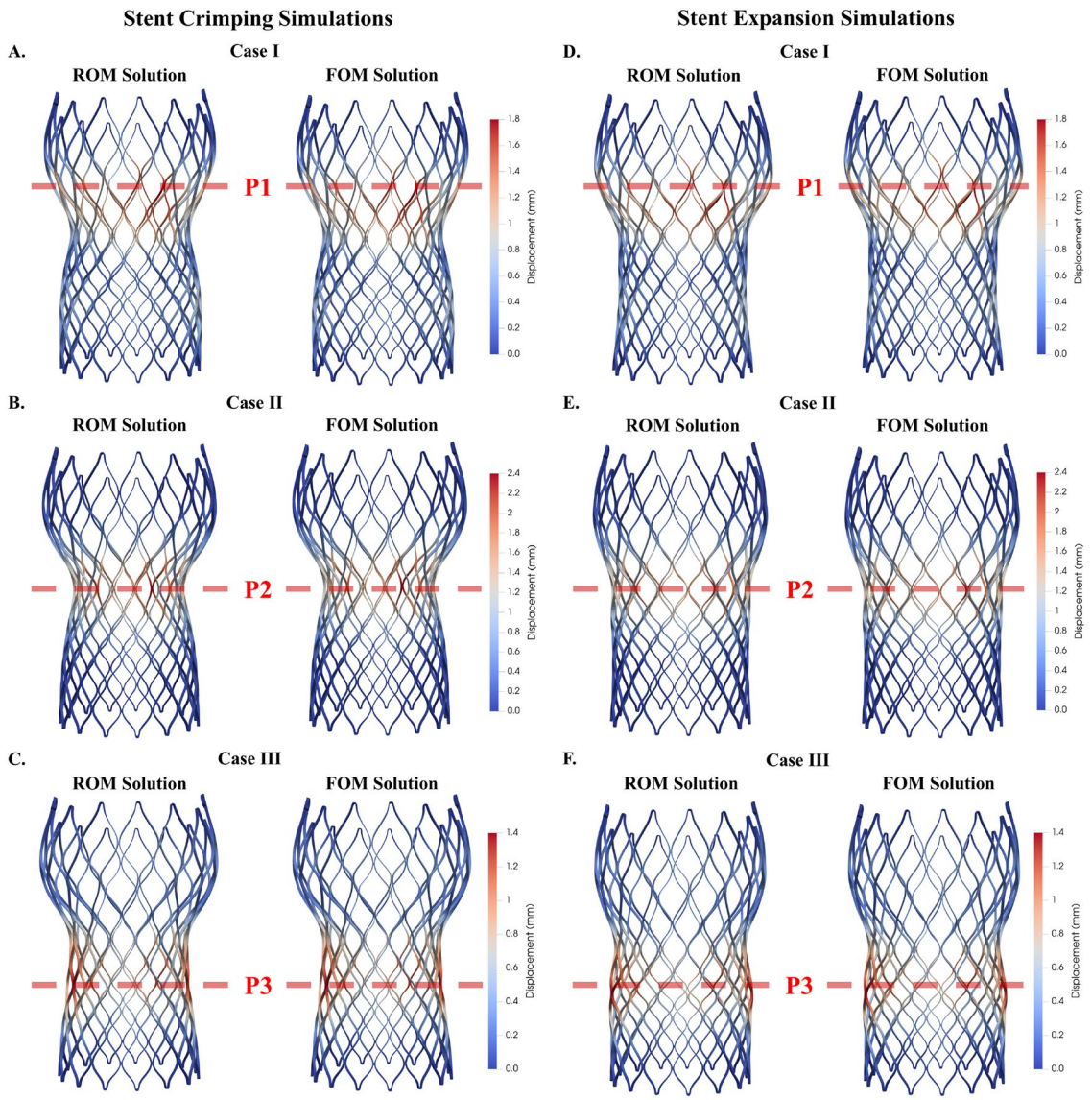

Fig. 4 Comparison between the stent deformation from the reduced order model (ROM) and the full order model (FOM) finite element simulations for the stent crimping (left: **A**–**C**) and expansion (right: **D**–**F**) scenarios at each of the three individual planes (P1, P2, P3) of the Evolut R stent. The stent deforms similarly between the two models in each case, where the maximum crimping is seen at each respective plane

number to be significantly smaller than for the FOM, with a consequent computational advantage.

With hyperelastic material properties, crimping simulations at all three planes using the ROM and FOM are shown in Fig. 7A. The maximum deformation in both the ROM and FOM simulations was 4.555 mm along P2, with similar deformations elsewhere. For the expansion case, the maximum deformation for both models was 4.538 mm along P2, with similar deformations for the rest of the stent frame (Fig. 7B). The number of reduced bases utilized in the online phase of the ROM was 20, a sharp reduction from the 210K degrees of freedom required for the FOM simulation. Average and relative errors for this case were similar in magnitude as shown previously.

Stress distributions for the linear and hyperelastic ROM simulations at all three planes are shown in Fig. 8. In the case of linear elastic simulations, the peak von Mises stress value occurs along the same planes at which the individual loads are directly applied (peak stress of 2344.66 kPa), while the stresses at all remaining areas of the stent frame are much lower and symmetrical along the frame's centerline. For the hyperelastic simulations, the stress values are much greater at all areas (peak stress of 9940.93 and 9692.11 kPa, respectively), and the highest stress values occur adjacent

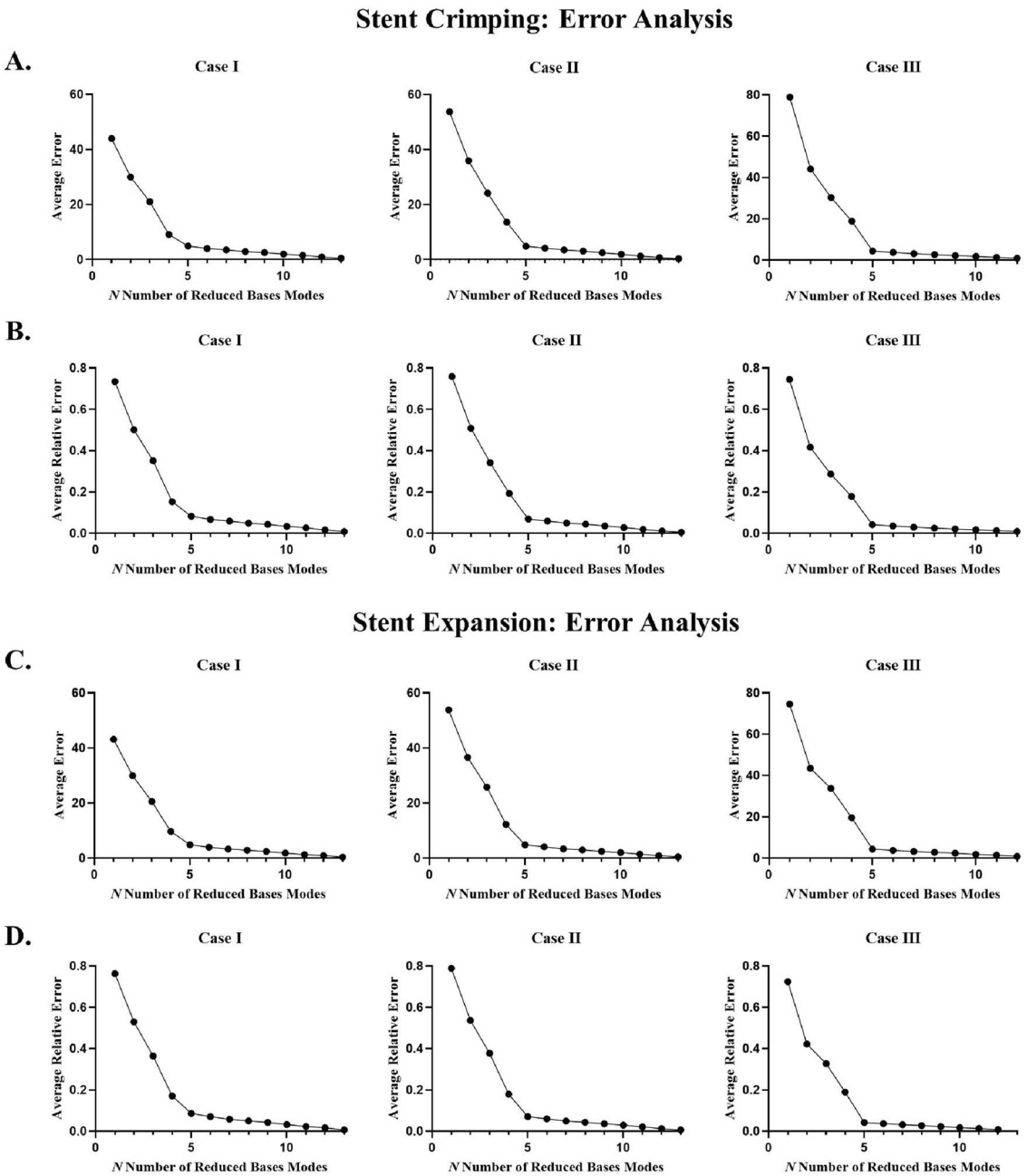

Fig. 5 Average error and relative error between the ROM and FOM simulations for the stent crimping (**A**, **B**) and expansion (**C**, **D**) simulations in each of the three cases (P1, P2, P3) calculated over the reduced bases *N* utilized in the model reduction

to the nodes at which the loads are applied. In addition, the stress distribution is more asymmetric as compared to the linear elastic results, with higher values near the force-pair nodes.

The computational details for the ROM and the FOM simulations are summarized in Table 1. FOM simulations required 210,417 degrees of freedom, while nearly all of the linear elastic ROM simulations utilized only 13 reduced bases to calculate the online solutions, except for the simulations along P3 which utilized 12, and simultaneous simulations along all planes which utilized 15 reduced bases. Simulating the linear elastic FOM solution required an average of 14.822 s. The total computational time for the linear elastic ROM offline phase was 1556.32 s, while the single parameter simulation performed in the online phase of the ROM took only an average of 1.045 s, a speed-up of 1489 times (relative to the offline phase), and a 92.9% decrease in computational costs as compared to the FE simulation. For

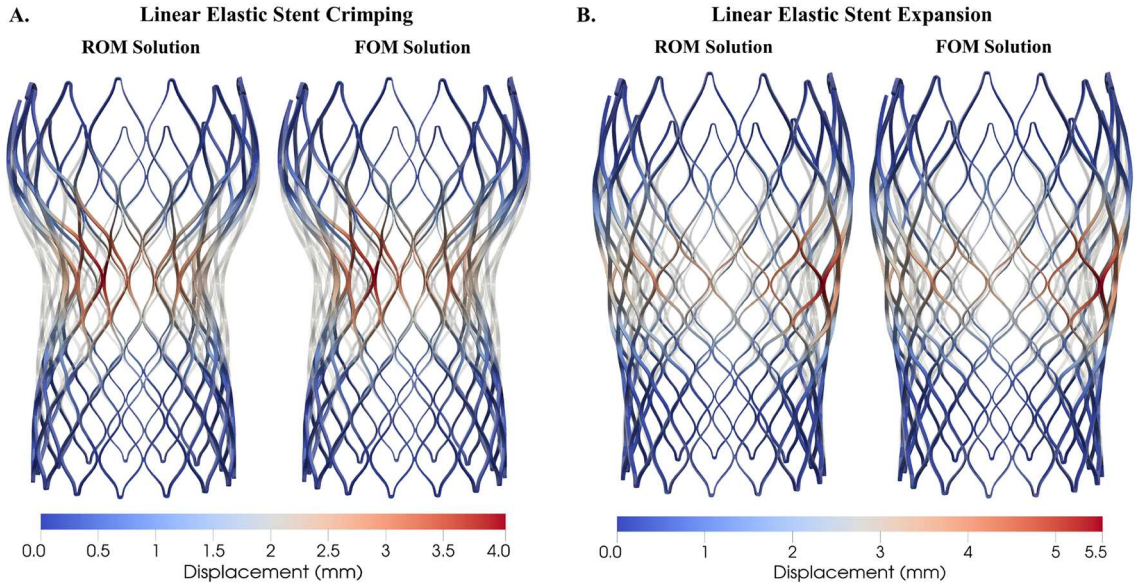

Fig. 6 Comparison between the stent deformation from the ROM and FOM simulations after performing linear elastic stent crimping (**A**) and expansion (**B**) simulations at all three planes simultaneously. The undeformed stent frame is overlaid in gray for reference. In both the expansion and crimping stages, the FOM and ROM feature similar solutions

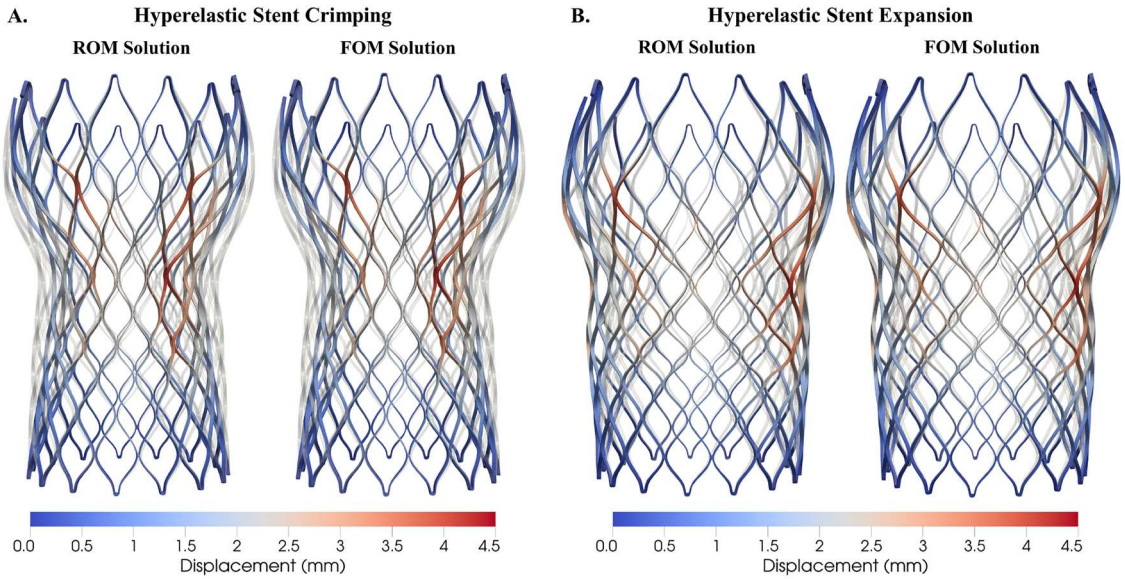

Fig. 7 Stent deformation from the hyperelastic ROM and FOM simulations after simulating stent crimping and expansion at all three planes simultaneously (**A** and **B**, respectively), with the undeformed stent geometry overlaid in gray for reference. The FOM and ROM again feature similar solutions for both sets of simulations

hyperelasticity, the ROM simulations required 20 reduced bases to calculate the online solution. This translated to an average computation time of 1.325 s in the online phase, compared to an average of 107.99 s for the hyperelastic FOM simulation, resulting in a speed-up factor of 81.50 (98.8% decrease in costs). In the case of the time-dependent hyperelastic simulations, the resultant deformations were identical to the previously shown hyperelastic results, and thus these results were not shown. An animation of the time-dependent displacement is shown in the supplemental materials for reference (Supplemental Video 1). In terms of computational times, the FE simulation required an average

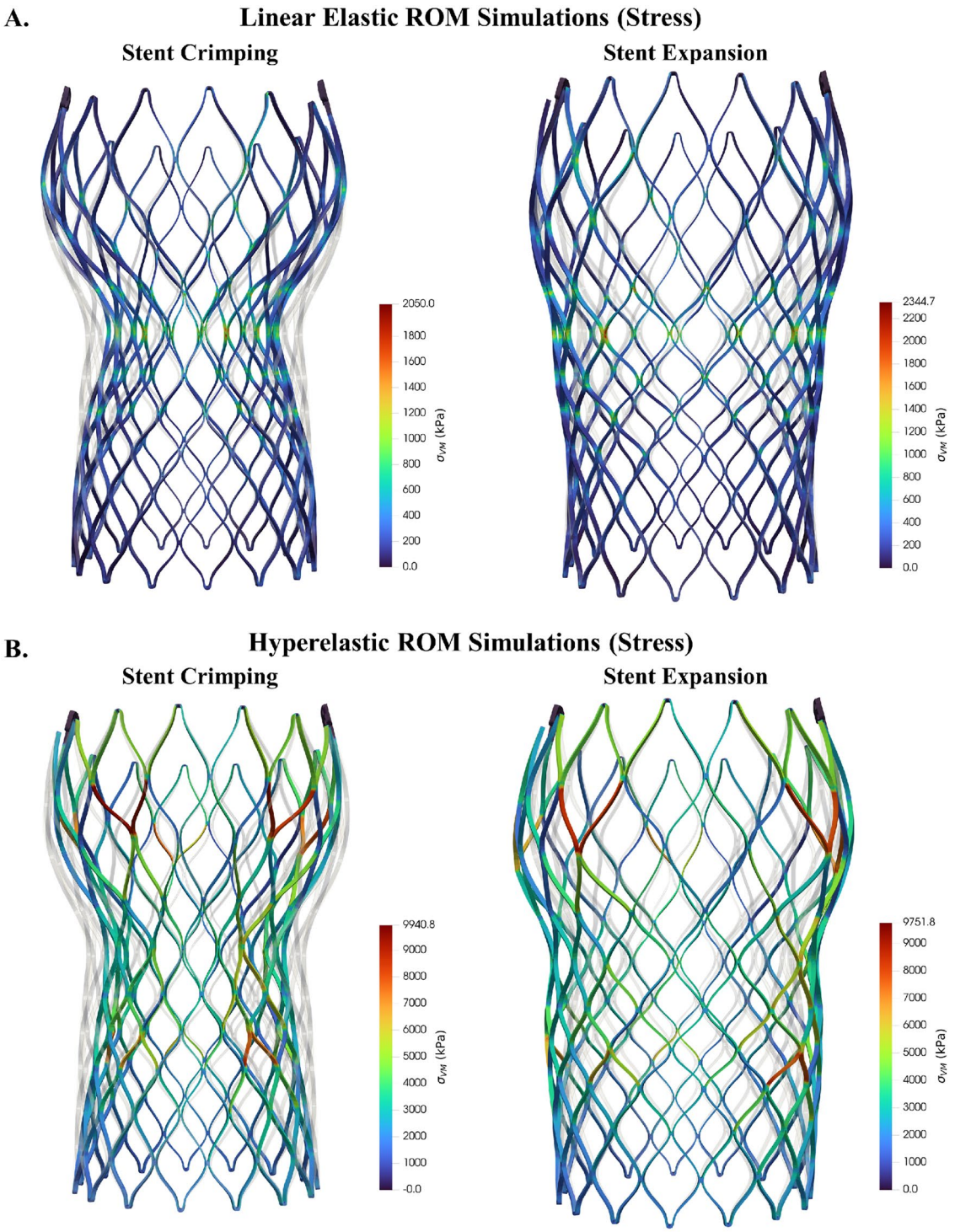

Fig. 8 Visualization of von Mises stress distribution from the linear elastic (**A**) and hyperelastic (**B**) ROM simulations, with the undeformed stent overlaid in gray for reference. Global and local differences can be seen between the two sets of crimping and expansion simulations in terms of resulting deformation pattern and stress magnitude

of 303.712 s to complete, while the online ROM simulation only required 21.828 s to complete, showing a strong reduction in the computational time with the use of the framework as well (92.8% decrease). We stress that the offline phase is done one for all, and does not affect the computational cost of all the subsequent online simulations, regardless of how many are needed.

Table 1 Summary of the computational details for all ROM and FOM FE simulations

Simulation	Mesh size	# of snapshots	# of FE DOF	# of RB	Wall clock time		
					FE (s)	ROM (online) (s)	ROM (offline) (h)
Linear elastic (POD)	270,715	105	210,417	12, 13, 15	14.82	1.045	0.43
Hyperelasticity (POD-DEIM)	270,715	105	210,417	20	107.991	1.325	72
Transient + hyperelasticity (POD-DEIM)	270,715	105	210,417	20	303.712	21.828	76

Discussion

In this *in-silico* study, we introduce a reduced order modeling framework applied toward rapidly simulating small structural deformations of the Evolut R stent frame. Beginning with the linear elastic offline stage simulations, a significant decay was seen in the eigenvalues of the snapshot library, which suggests that creating the reduced basis functions from 13 principal components would sufficiently capture the information from the FE snapshot library. Similarly, in both the steady and transient hyperelastic cases, a decay in the eigenvalues was seen after 20 reduced bases, indicating that this would be sufficient for further model reduction. The difference in reduced bases between the two cases is expected, as the nonlinear problem requires additional information from the snapshot library to accurately perform the online phase. Utilizing the POD-Galerkin approach coupled with DEIM for treatment of the nonlinear terms resulted in a reduced order solution that was equivalent to the FE simulation with the same set of newly applied parameters (average percent error less than 3%). The ROM simulation required significantly less computational time compared to the FOM FE simulation in all cases, suggesting that the POD-Galerkin-based ROM results in an accurate and computationally efficient solution as compared to conventional FE methods. Most promisingly, this was especially evident in the time-dependent hyperelastic problem, where the use of the POD-DEIM approach resulted in the simulation of a transient deformation process with time-dependent BCs that was completed in under 30 s.

These preliminary findings are especially encouraging for performing the full deployment process in the future, where the current framework can be readily adapted to capture such a scenario. For example, separate ROMs may be constructed using the applied force-pairs to first fully crimp the stent, and then deploy the crimped stent into its natural position. Coupling these frameworks would then allow the user to replicate the entire TAVR deployment within a patient-specific context. We anticipate a significant role of ROMs in segregated algorithms for such solid–solid or fluid–structure interactions (steady or transient). Segregated algorithms generally rely on iterative procedures where each subproblem (e.g., structure or fluid) is solved several times until the fulfillment of a convergence requirement, and when using the FOM, this clearly reflects in a high computational cost. When referring the offline phase to a reference geometry, eventually to be mapped into the current one, POD seems to be the ideal tool for dramatically accelerating segregated algorithms, thus making them a viable option for extensive simulation campaigns.

Computational Models for TAVR Deployment Structural analysis of THVs has become an increasingly common area of focus in better understanding the physiological interactions between the valve and the native aortic geometry. Numerous *in-silico* studies have shown the importance of radial forces applied on the aortic annulus from self-expandable valves, such as the Evolut R, during the TAVR deployment procedure, as well as the significance of arterial wall deformation in response to the TAVR deployment [35, 53]. The deformation magnitude of the Evolut R stent frame in response to the various applied loads in this study resembles those found in these previous *in-silico* studies [29, 53]. Additionally, the deformations shown here are similar to those found in clinical studies analyzing the degree of post-implantation prosthesis deformation, which can be caused by asymmetric leaflet expansion or development of large calcium deposits, and may be associated with complications such as Hypo-Attenuating Leaflet Thickening (HALT) [28].

Importantly, the desired deformations can be easily achieved using the online phase of the ROM to match either smaller or larger (with appropriate superelastic properties) magnitudes seen in the literature, all at extremely low computational costs. The numerical experiments reported here, where the radial loads are primarily applied at nodes located across P1, P2, and P3 of the stent frame, resulted in idealized deformations that may serve as an initial approximation of the deformation of the stent in response to potential loads from the aortic wall, prosthetic valve leaflets, and calcium deposits. When comparing the linear and hyperelastic simulations presented, the displacements between the two cases are largely similar, suggesting that the linear elastic model is a valid approximation of the nonlinear case for such small displacement regimes. The stent frame deforms symmetrically around the loads applied in both cases, with small

differences in the curved nature of the final deformed shape. These similarities between the two simulations are expected when the displacement regime is small (1-3 mm). However, we expect significant differences at larger displacement regimes, such as those that the Evolut R valve experiences when it is fully crimped and deployed.

Several studies have also explored the deployment mechanics of balloon-expandable THV devices, such as the Edwards SAPIEN valve [14, 53]. Although the framework developed here began with a focus on self-expandable THVs, it may serve as a starting point for performing real-time deployment simulations of balloon-expandable valves as well, where the only input required would be the 3D geometry and meshes of the device of interest. In terms of material properties, these devices are most often modeled with an elastoplastic constitutive model, which can be readily implemented within the *FEniCS* and *RBniCS* solvers used here. Precise care must be taken, however, with regard to the applied loading conditions and the locations at which they are applied, as the force-pairs described here must be adapted to accurately reflect the effects of the balloon expansion.

Role of ROMs in TAVR Modeling Conventional FE methods used to model and predict pre-operative TAVR deployment require a large number of degrees of freedom, and in turn extremely large computation times (up to 48-96 h). Predicting the effects of various valve types and configurations for a single patient may require multiple simulations, which thus requires several days to weeks to complete and becomes unfeasible for the clinical environment in which rapid and accurate predictive models are required. To this end, artificial intelligence-based simulation technology such as those developed by FEops (FEops HEARTguide, Ghent, Belgium) utilizes a *data-driven* approach toward providing real-time simulations in the clinic. However, this is in contrast to *model-driven* approaches such as the ROMs presented here, which directly utilize and preserve the classical mechanics that govern such structural problems, and do not rely on large sets of clinical data that may not be readily available for predictive uses.

As evidenced by the results shown, utilizing *model-driven* approaches like ROMs allows for a significant reduction in the computational costs as well (Table 1). These computational savings may be especially practical for simulating TAVR deployment in the clinic, as ROMs allow for a one-time offline phase followed by the opportunity to use a variety of different parameters that provide accurate and computationally cheap results. In the setting of full TAVR deployment, these parameters may include valve positioning within a patient-specific aortic root, different material properties of the valve, or geometrical parametrization of different valve sizes and types [27, 46]. In such cases, an optimization framework using the aforementioned parameters can be developed that leverages the ROM framework, allowing for real-time optimization simulations for individual patients. In fact, previous studies have looked at optimization of THV sizing and positioning, as well as design and optimization of new THVs all via computational modeling [25, 32, 38]. Conversely, other *data-driven* techniques such as surrogate modeling have also been used previously for performing these optimizations in a rapid manner, specifically for the design of the THV stent frame geometries [9, 17]. ROMs may play a pivotal role in such cases to reduce the computational costs of performing these optimization simulations in a *model-driven* fashion, preserving the underlying mechanics of the governing problem.

These savings in computational costs are based on the reduction of the degrees of freedom in the reduced order problem. For all FOM simulations shown here, there were 210,417 degrees of freedom. In the reduced order problem, this was simplified to 12, 13, and 15 reduced bases depending on the specific case for the linear elastic simulations, and 20 reduced basis for the hyperelastic, which translates to a much simpler system of equation that must be solved. Specifically, the size of the matrix $W^T AW$ from Eq. (9) becomes 12×12, 13×13, 15×15, or 20×20, depending on the simulated case, to compare with the FE matrix A from (8) (210,417 by 210,417). The savings in computational costs thus become evident. However, there is a limit for these savings, namely with nonlinear time-dependent problems. In such problems, the POD-Galerkin approach works to reduce the number of variables present, but does not reduce the complexity of assembling the nonlinear terms of the governing problem [21]. Thus, these terms would be assembled inefficiently in the online phase of the ROM with the traditional POD-Galerkin method. To this end, more advanced model reduction techniques such as DEIM allow for streamlined model reduction of the nonlinear terms to create the reduced bases, and when coupled with the standard POD-Galerkin approach, they result in extremely efficient computational simulations as evidenced by Table 1.

Offline Phase of the ROM It should be emphasized that the offline phase of the ROM is relatively computationally expensive even compared to the FOM simulations. In simulating the linear elastic deformation of the valve frame, this expense may seem unnecessary and a hindrance. However, the offline phase is a one-time procedure composed of several FE simulations. For full TAVR deployment analysis, these individual FE simulations require more advanced time-dependent constitutive models such as superelasticity, a multitude of parameters, unique boundary conditions, and dense meshes that results in extremely expensive individual simulations. The offline phase of the ROM for these complex cases would require even more computation time, especially when using DEIM, as the secondary evaluations of the nonlinear terms require additional time and memory to perform.

However, the online phase of the ROM would then reduce these expenses by an even larger factor, as evidenced by the hyperelastic ROM simulations shown here. This trade-off is especially beneficial for segregated algorithms in clinical settings. In such cases, the offline phase may be offloaded to high-performance computing clusters, where the availability of memory and the use of parallel computing would enable faster computations of the required snapshot libraries and reduced basis functions. In turn, the online phase of the ROM would enable the user to rapidly produce complex predictive models in a real-time setting that would otherwise take several days or weeks to complete, all on local computational facilities.

Study Limitations and Future Work

The findings shown here should be interpreted in the context of several limitations. One essential limitation is that the Evolut R stent frame was modeled as a linear elastic and hyperelastic material. Using these constitutive models limits the degree to which the ROM framework can accurately deform the stent frame at larger displacement regimes and provide physiologically relevant parameters (stresses, strains, pullout forces, etc.). Namely the stresses and displacements shown here are markedly lower than those in traditional TAVR computational studies. Although the framework shows promising results for nonlinear constitutive laws, the self-expandable nitinol frame of the valve in reality would be more accurately modeled as a superelastic alloy, especially for large deformations seen in traditional crimping and deployment simulations [4, 41, 55]. Thus, a constitutive model for superelasticity is needed, such as suggested by Auricchio et al. [5] With a superelastic model, full crimping and deployment simulations can be performed via the ROM framework, resulting in physiologically accurate deformations and stresses.

To extend the ROM framework to more practical transient nonlinear problems (i.e., traditional numerical simulation of the TAVR deployment process), more precise boundary conditions will be required as well. During traditional numerical simulations of TAVR, the crimping and expansion process occurs uniformly along the entire stent frame using a cylindrical catheter, which is not captured with the current conditions employed [13, 30]. Moving forward, the aortic root geometry will be needed to replicate the full crimping and deployment simulations, where the force-pair loads introduced in this study will be essential for replicating the use of the cylindrical catheter. Even following implantation of the THV, the valve frame may not be completely fixed in physiological conditions due to varying laminar and oscillatory shear stress environments as well as loads applied from the prosthetic leaflets and developing calcium deposits [7, 57]. Thus, the homogenous Dirichlet boundary conditions applied at the extreme edges of the stent assume may need to be modified to accurately capture the post-implantation valve dynamics. For this study though, these assumptions hold valid as the primary objective was to analyze the applicability and effectiveness of the POD-Galerkin-based ROM.

Future work includes incorporating the superelastic material properties of the nitinol stent frame, as well as replicating the fully realistic crimping and deployment process in patient-specific aortic root geometries, potentially via the coupling of separate ROM libraries as mentioned previously. Such a deployment process will also require appropriately defined contact mechanics at the stent frame-aortic root interface. Implementation of the contact problem will be explored via a domain-decomposition and momentum exchange approach, and when integrated into the ROM framework, will allow for real-time contact simulations as well [10]. In addition, we plan to incorporate the pericardium leaflets of the Evolut R valve to the model utilized here. Separate ROM frameworks will then be developed for valve leaflet deformation in response to applied hemodynamic loads during the cardiac cycle (CC), and for flow through the valve leaflets at varying points along the CC. The long-term goal is to couple the aforementioned ROM frameworks that tackle the structural part of the TAVR deployment process with ROMs that addresses the fluid dynamic problem during and post-implantation, resulting in a comprehensive framework that can provide accurate and rapid results both in the structural and fluid domains.

Conclusion

In this study, we introduce a POD-Galerkin-based ROM framework applied in the structural deformation of the 26 mm Medtronic Evolut R valve. With the use of this framework, we have shown significant decreases in the computation time for simulating steady, transient, and nonlinear elastic deformation problems using the Evolut R stent frame. In addition to the reduced computational costs, the ROM simulations also resulted in solutions that were nearly identical to traditional FE methods employed to simulate similar idealized radial deformations of the stent frame. Further refinements of the ROM framework are underway to rapidly and accurately simulate the TAVR deployment process in its entirety, as well as the fluid dynamic interactions of the THV with the surrounding aortic geometries.

Supplementary Information The online version contains supplementary material available at https://doi.org/10.1007/s10439-023-03360-5.

Acknowledgements The authors would like to acknowledge Gianluigi Rozza (SISSA, Trieste, Italy) for his scientific guidance in the development of the *RBniCS* project. We also acknowledge all members of the Cardiovascular Fluid Mechanics (CFM) Lab at the Georgia

Institute of Technology as well as the Emory Center for Mathematics and Computing in Medicine at Emory University for their support. The research reported was supported by the NSF under Award Number DMS2012286 (PI: A. Veneziani with O. San and T. Iliescu). FB thanks the project "Reduced order modelling for numerical simulation of partial differential equations" funded by Università Cattolica del Sacro Cuore, and the INDAM-GNCS project "Metodi numerici per lo studio di strutture geometriche parametriche complesse" (CUP_E53C22001930001, PI Dr. Maria Strazzullo).

Declarations

Conflict of interest The authors have no conflict of interest to disclose with the research presented here.

References

1. Ahrens, J., B. Geveci, and C. Law. Paraview: an end-user tool for large data visualization. *Vis. Handb.* 717:500381, 2005.
2. Alnæs, M., J. Blechta, J. Hake, A. Johansson, B. Kehlet, A. Logg, C. Richardson, J. Ring, M. E. Rognes, and G. N. Wells. The Fenics project version 15. *Arch. Numer. Softw.* 3:100, 2015.
3. Anam, S., B. Kovarovic, R. Ghosh, M. Bianchi, A. Hamdan, R. Haj-Ali, and D. Bluestein. Assessment of paravalvular leak severity and thrombogenic potential in transcatheter bicuspid aortic valve replacements using patient-specific computational modeling. *J. Cardiovasc. Transl. Res.* 15:834–844, 2021.
4. Auricchio, F., M. Conti, S. Morganti, and A. Reali. Simulation of transcatheter aortic valve implantation: a patient-specific finite element approach. *Comput. Methods Biomech. Biomed. Eng.* 17:1347–1357, 2013.
5. Auricchio, F., R. L. Taylor, and J. Lubliner. Shape-memory alloys: macromodelling and numerical simulations of the superelastic behavior. *Comput. Methods Appl. Mech. Eng.* 146:281–312, 1997.
6. Bailoor, S., J.-H. Seo, L. Dasi, S. Schena, and R. Mittal. A computational study of the hemodynamics of bioprosthetic aortic valves with reduced leaflet motion. *J. Biomech.* 120:110350, 2021.
7. Balachandran, K., P. Sucosky, and A. P. Yoganathan. Hemodynamics and mechanobiology of aortic valve inflammation and calcification. *Int. J. Inflamm.* 2011. https://doi.org/10.4061/2011/263870.
8. Ballarin, F., E. Faggiano, A. Manzoni, A. Quarteroni, G. Rozza, S. Ippolito, C. Antona, and R. Scrofani. Numerical modeling of hemodynamics scenarios of patient-specific coronary artery bypass grafts. *Biomech. Model. Mechanobiol.* 16:1373–1399, 2017.
9. Barati, S., N. Fatouraee, M. Nabaei, F. Berti, L. Petrini, F. Migliavacca, and J. F. R. Mata. A computational optimization study of a self-expandable transcatheter aortic valve. *Comput. Biol. Med.* 139:104942, 2021.
10. Barboteu, M., P. Alart, and M. Vidrascu. A domain decomposition approach strategy for nonclassical frictional multi-contact problems. *Comput. Methods Appl. Mech. Eng.* 190:37–38, 2001.
11. Barrault, M., Y. Maday, N. C. Nguyen, and A. T. Patera. An 'empirical interpolation' method: application to efficient reduced-basis discretization of partial differential equations. *C.R. Math.* 339:667–672, 2004.
12. Bertagna, L., and A. Veneziani. A model reduction approach for the variational estimation of vascular compliance by solving an inverse fluid-structure interaction problem. *Inverse Prob.*30:055006, 2014.
13. Bianchi, M., R. P. Ghosh, G. Marom, M. J. Slepian, and D. Bluestein. Simulation of transcatheter aortic valve replacement in patient-specific aortic roots: effect of crimping and positioning on device performance. In: 2015 37th Annual International Conference of the IEEE Engineering in Medicine and Biology Society (EMBC), pp. 282–285, IEEE2015.
14. Bianchi, M., G. Marom, R. P. Ghosh, O. M. Rotman, P. Parikh, L. Gruberg, and D. Bluestein. Patient-specific simulation of transcatheter aortic valve replacement: impact of deployment options on paravalvular leakage. *Biomech. Model. Mechanobiol.* 18:435–451, 2019.
15. Brown, J., J. Lee, M. Smith, D. Wells, A. Barrett, C. Puelz, J. Vavalle, and B. Griffith. Patient-specific immersed finite element-difference model of transcatheter aortic valve replacement. *Ann. Biomed. Eng.* 51:103–116, 2023.
16. Capelli, C., G. M. Bosi, E. Cerri, J. Nordmeyer, T. Odenwald, P. Bonhoeffer, F. Migliavacca, A. M. Taylor, and S. Schievano. Patient-specific simulations of transcatheter aortic valve stent implantation. *Med. Biol. Eng. Comput.* 50:183–192, 2012.
17. Carbonaro, D., D. Gallo, U. Morbiducci, A. Audenino, and C. Chiastra. In silico biomechanical design of the metal frame of transcatheter aortic valves: multi-objective shape and cross-sectional size optimization. *Struct. Multidiscip. Optim.* 64:1825–1842, 2021.
18. Carbonaro, D., S. Zambon, A. Corti, D. Gallo, U. Morbiducci, A. Audenino, and C. Chiastra. Impact of nickel-titanium superelastic material properties on the mechanical performance of self-expandable transcatheter aortic valves. *J. Mech. Behav. Biomed. Mater.*138:105623, 2023.
19. Chakravarty, T., L. Søndergaard, J. Friedman, O. De Backer, D. Berman, K. F. Kofoed, H. Jilaihawi, T. Shiota, Y. Abramowitz, T. H. Jørgensen, et al. Subclinical leaflet thrombosis in surgical and transcatheter bioprosthetic aortic valves: an observational study. *Lancet*. 389:2383–2392, 2017.
20. Chatterjee, A. An introduction to the proper orthogonal decomposition. *Curr. Sci.* 78:808–817, 2000.
21. Chaturantabut, S., and D. Sorensen. Discrete empirical interpolation for nonlinear model reduction. In: Proceedings of the 48th IEEE Conference on Decision and Control (CDC), pp. 4316–4321, 2009.
22. Cueto, E., and F. Chinesta. Real time simulations for computational surgery: a review. *Adv. Model. Simul. Eng. Sci.* 1:1–18, 2014.
23. Dasi, L. P., H. Hatoum, A. Kheradvar, R. Zareian, S. H. Alavi, W. Sun, C. Matin, T. Pham, Q. Wang, V. Raghav, and A. P. Yoganathan. On the mechanics of transcatheter aortic valve replacement. *Ann. Biomed. Eng.* 45:310–331, 2017.
24. Daubert, M. A., N. J. Weissman, R. T. Hahn, P. Pibarot, R. Parvataneni, M. J. Mack, L. G. Svensson, D. Gopal, S. Kapadia, R. J. Siegel, et al. Long-term valve performance of TAVR and SAVR: a report from the partner I trial. *Cardiovasc. Imaging*. 10:15–25, 2017.
25. Dowling, C., R. Gooley, L. McCormick, S. Brecker, S. Firoozi, V. Bapat, S. Kodali, O. Khalique, J. Brouwer, and M. Swaans. Patient-specific computer simulation to optimize transcatheter heart valve sizing and positioning in bicuspid aortic valve. *Struct. Heart*. 5:621–630, 2021.
26. Esmailie, F., A. Razavi, B. Yeats, S. K. Sivakumar, H. Chen, M. Samaee, I. Shah, A. Veneziani, P. Yadav, V. Thourani, and L. P. Dasi. Biomechanics of transcatheter aortic valve replacement complications and computational predictive modeling. *Struct. Heart*.6:100032, 2022.
27. Finotello, A., S. Morganti, and F. Auricchio. Finite element analysis of TAVI: impact of native aortic root computational modeling strategies on simulation outcomes. *Med. Eng. Phys.* 47:2–12, 2017.
28. Fukui, M., V. Bapat, S. Garcia, M. Dworak, G. Hashimoto, H. Sato, M. Gossl, M. Enriquez-Sarano, J. Lesser, J. Cavalcante, and

P. Sorajja. Deformation of transcatheter aortic valve prosthesis: Implications for hypoattenuating leaflet thickening and clinical outcomes. *Circulation*. 146:480–493, 2022.
29. Gessat, M., R. Hopf, T. Pollok, C. Russ, T. Frauenfelder, S. Sundermann, S. Hirsch, E. Mazza, G. Szekely, and V. Falk. Image-based mechanical analysis of stent deformation: concept and exemplary implementation for aortic valve stents. *IEEE Trans. Biomed. Eng.* 61:4–15, 2013.
30. Gunning, P. S., T. J. Vaughan, and L. M. McNamara. Simulation of self expanding transcatheter aortic valve in a realistic aortic root: implications of deployment geometry on leaflet deformation. *Ann. Biomed. Eng.* 42:1989–2001, 2014.
31. Hall, G., and E. Kasper. Comparison of element technologies for modeling stent expansion. *J. Biomech. Eng.* 128:751–756, 2006.
32. Helbock, R., S. Anam, B. Kovarovic, M. Slepia, A. Hamdan, R. Haj-Ali, and D. Bluestein. Designing a novel asymmetric transcatheter aortic valve for stenotic bicuspid aortic valves using patient-specific computational modeling. *Ann. Biomed. Eng.* 51:58–70, 2022.
33. Hesthaven, J. S., G. Rozza, B. Stamm, et al. Certified Reduced Basis Methods for Parameterized Partial Differential Equations, Vol. 590, Berlin: Springer, 2016.
34. Heywood, J. G., R. Rannacher, and S. Turek. Artificial boundaries and flux and pressure conditions for the incompressible Navier-Stokes equations. *Int. J. Numer. Meth. Fluids*. 22:325–352, 1996.
35. Hsu, M.-C., D. Kamensky, Y. Bazilevs, M. S. Sacks, and T. J. Hughes. Fluid-structure interaction analysis of bioprosthetic heart valves: significance of arterial wall deformation. *Comput. Mech.* 54:1055–1071, 2014.
36. Kandail, H., S. Trivedi, A. Shaikh, T. Bajwa, D. O'Hair, A. Jahangir, and J. LaDisa. Impact of annular and supra-annular CoreValve deployment locations on aortic and coronary artery hemodynamics. *J. Mech. Behav. Biomed. Mater.* 86:131–142, 2018.
37. Kodali, S. K., M. R. Williams, C. R. Smith, L. G. Svensson, J. G. Webb, R. R. Makkar, G. P. Fontana, T. M. Dewey, V. H. Thourani, A. D. Pichard, et al. Two-year outcomes after transcatheter or surgical aortic-valve replacement. *N. Engl. J. Med.* 366:1686–1695, 2012.
38. Kovarovic, B., R. Helbock, K. Baylous, O. Rotman, M. Slepian, and D. Bluestein. Visions of TAVR future: development and optimization of a second generation novel polymeric TAVR. *J. Biomech. Eng.*144:061008, 2022.
39. Lavon, K., G. Marom, M. Bianchi, R. Halevi, A. Hamdan, A. Morany, E. Raanani, D. Bluestein, and R. Haj-Ali. Biomechanical modeling of transcatheter aortic valve replacement in a stenotic bicuspid aortic valve: deployments and paravalvular leakage. *Med. Biol. Eng. Comput.* 57:2129–2143, 2019.
40. Logg, A., K.-A. Mardal, and G. Wells. Automated Solution of Differential Equations by the Finite Element Method: The FEniCS Book, Vol. 84, Berlin: Springer, 2012.
41. Luraghi, G., F. Migliavacca, A. Garcia-Gonzalez, C. Chiastra, A. Rossi, D. Cao, G. Stefanini, and J. F. R. Matas. On the modeling of patient-specific transcatheter aortic valve replacement: a fluid-structure interaction approach. *Cardiovasc. Eng. Technol.* 10:437–455, 2019.
42. Luraghi, G., J. F. R. Matas, and F. Migliavacca. In silico approaches for transcatheter aortic valve replacement inspection. *Expert Rev. Cardiovasc. Therapy*. 19:61–70, 2020.
43. Mao, W., Q. Wang, S. Kodali, and W. Sun. Numerical parametric study of paravalvular leak following a transcatheter aortic valve deployment into a patient-specific aortic root. *J. Biomech. Eng.*140:101007, 2018.
44. Midha, P., V. Raghav, J. Condado, I. Okafor, S. Lerakis, V. Thourani, V. Babaliaros, and A. Yoganathan. Valve type, size, and deployment location affect hemodynamics in an in vitro valve-in-valve model. *Cardiovasc. Interv.* 9:1618–1628, 2016.
45. Mmg-Open-Source-Consortium. https://github.com/MmgTools/mmg.
46. Morganti, S., N. Brambilla, A. Petronio, A. Reali, F. Bedogni, and F. Auricchio. Prediction of patient-specific post-operative outcomes of TAVI procedure: the impact of the positioning strategy on valve performance. *J. Biomech.* 49:2513–2519, 2016.
47. Mummert, J., E. Sirois, and W. Sun. Quantification of biomechanical interaction of transcatheter aortic valve stent deployed in porcine and ovine hearts. *Ann. Biomed. Eng.* 41:577–586, 2012.
48. Padala, M., E. L. Sarin, P. Willis, V. Babaliaros, P. Block, R. A. Guyton, and V. H. Thourani. An engineering review of transcatheter aortic valve technologies. *Cardiovasc. Eng. Technol.* 1:77–87, 2010.
49. Pfaller, M. R., M. C. Varona, J. Lang, C. Bertoglio, and W. A. Wall. Using parametric model order reduction for inverse analysis of large nonlinear cardiac simulations. *Int. J. Numer. Methods Biomed. Eng.*36:e3320, 2020.
50. Quarteroni, A., R. Sacco, and F. Saleri. Numerical Mathematics, Vol. 37, Berlin: Springer, 2010.
51. Ribeiro, H. B., L. Nombela-Franco, M. Urena, M. Mok, S. Pasian, D. Doyle, R. DeLarochellière, M. Côté, L. Laflamme, H. DeLarochellière, et al. Coronary obstruction following transcatheter aortic valve implantation: a systematic review. *Cardiovasc. Interv.* 6:452–461, 2013.
52. Schneider, T., Y. Hu, X. Gao, J. Dumas, D. Zorin, and D. Panozzo. A large-scale comparison of tetrahedral and hexahedral elements for solving elliptic PDEs with the finite element method. *ACM Trans. Graph.* 41:1–14, 2022.
53. Tzamtzis, S., J. Viquerat, J. Yap, M. Mullen, and G. Burriesci. Numerical analysis of the radial force produced by the medtronic-corevalve and edwards-sapien after transcatheter aortic valve implantation (TAVI). *Med. Eng. Phys.* 35:125–130, 2013.
54. Van Loan, C. F., and G. Golub. Matrix Computations. Johns Hopkins Studies in Mathematical Sciences. Baltimore: The Johns Hopkins University Press, 1996.
55. Wang, Q., E. Sirois, and W. Sun. Patient-specific modeling of biomechanical interaction in transcatheter aortic valve deployment. *J. Biomech.* 45:1965–1971, 2012.
56. Yang, H., and A. Veneziani. Efficient estimation of cardiac conductivities via POD-DEIM model order reduction. *Appl. Numer. Math.* 115:180–199, 2017.
57. Yap, C. H., N. Saikrishnan, G. Tamilselvan, and A. P. Yoganathan. Experimental measurement of dynamic fluid shear stress on the aortic surface of the aortic valve leaflet. *Biomech. Model. Mechanobiol.* 11:171–182, 2012.
58. Zainib, Z., F. Ballarin, S. Fremes, P. Triverio, L. Jiménez-Juan, and G. Rozza. Reduced order methods for parametric optimal flow control in coronary bypass grafts, toward patient-specific data assimilation. *Int. J. Numer. Methods Biomed. Eng.*37:e3367, 2020.